VOL. 15, NO. 19, OCTOBER 2020 ISSN 1819-6608
ARPN Journal of Engineering and Applied Sciences

www.arpnjournals.com

OFF-DESIGN PERFORMANCE OF AUTOMOTIVE DERIVED CENTRIFUGAL COMPRESSORS

Luca Piancastelli[1], Federico Calzini[2] and Stefano Cassani[2]
[1]Department of Industrial Engineering, Alma Mater Studiorum University of Bologna, Viale Risorgimento, Bologna, Italy
[2]MultiProjecta, Via Casola Canina, Imola (BO), Italy
E-Mail: luca.piancastelli@unibo.it

ABSTRACT

The traditional method to draw automotive-turbocharger compressor maps is based on equivalent chocking conditions. In this way, theoretically, the compressor chocking conditions would be exactly evaluated with the new ambient (inlet) conditions. Unfortunately, chocking is not the worst working condition for turbochargers in piston engine applications. In addition, most available compressor maps are interpolated from very few CFD (Computational Fluid Dynamics) or experimental data. The result is that many designers convert the map into a "row" one with the volumetric max flow on the x-axis. However, even this approach has many limitations, since compressor performance depends on Mach and Re numbers. To clarify the concept, a simplified CFD method to draw the compressor map is introduced in this paper. An example, based on a true turbocharger, shows the limitations of most interpolated-maps that can be found in literature. This initial "raw" map has a volumetric flow rate in input (x-axis) and an absolute pressure ratio in output (y-axis). The islands of constant efficiency are then calculated by assuming that the diffuser has a unitary efficiency. Then a new method based on invariants is introduced to calculate the new map with different input ambient conditions [1]. It is based on the ambient sound speed. This method is then corrected in this paper by introducing more accurate values for density and Mach speed. In particular the correction due to the air moisture content is particularly critical. The new invariant map obtained in this way takes into account of variations in inlet air for Re and Mach numbers. The method is valid for automotive and aerospace applications up to 3,000m. Unfortunately, for higher altitudes, even this new method shows its limitations, with the necessity to recalculate the maps with CFD simulation. In fact, rarified air and lower inlet temperature reduce compressor performance in term of efficiency and compression ratio. On the contrary, turbines tend to transfer more power to the shaft. In this way, the compressor to turbine match is far from ideal.

Keywords: compressor, turbine, turbocharger, map, altitude, water content.

INTRODUCTION

Properly designed centrifugal compressors would never reach the same efficiency of the best axial ones. However, they are very popular in applications with low mass flow and the necessity of a stable and efficient off-design performance. This is the case of turbochargers for automotive piston engines. In this field the requirement of questionable emission reduction have compelled the designers to use only turbocharged piston engines. For this reason, an enormous research work has been done for the mass production of low-inertia and high efficiency units with centrifugal compressors shafted to a centripetal turbine. While turbine design is relatively simple due to the availability of an excessive amount of energy, the compressor design proved to be critical. A very wide map with a large difference between the lowest and the highest fluid flow is required. At the same time, especially for last generation Euro 6 diesel, high maximum pressure is also necessary to cope with all the restrictions on the intake and on the exhaust. At the same time, very small compressors/turbines are required to minimize polar inertia and turbolag. Compressor/turbine maps are often difficult to obtain even for large car manufacturers, especially for last generation turbochargers with VGTs (Variable Geometry Tubine) or variable intake. Even when they are available, they use normalized mass/flow in input with equations to be applied for different air conditions in input. The reason of this choice is beyond the scope of this paper; however, it should be clear that compressors are mostly volumetric machines. They work with a volume of air that is accelerated up to (absolute) supersonic flow at the exit of the compressor wheel (impeller). In fact, design methods with velocity triangles were commonly used in the past. Most of the papers are focused on the impeller design. In these papers, the reaction degree of the impeller is very small and, in many cases, a vaned diffuser is advised for best performance. In very high speed, low inertia automotive compressor, the vaned diffuser is difficult to implement efficiently. In almost all automotive cases, a vaneless diffuser decelerates the supersonic high speed from the impeller to a subsonic value. Even if many Authors advice to use vaned diffusers for the best efficiency in transforming the velocity into pressure, the Authors found that this fact is only marginally true. In addition, this concept is valid only for the compressor design point. If inlet ambient conditions and flow requirement vary, the vanes hugely reduce the off-design efficiency. Therefore, it is doubtful that the use of a vaned diffuser is cost-effective. In the range of automotive turbochargers compressor ratio (2:1-5:1), the commercial diffusers are vaneless. Another large discrepancy between literature and Authors findings comes from the fact that impeller design is much easier than diffuser design. While impeller design is relatively easy with modern CAE (Computer Aided Engineering) tools, the diffuser is still difficult to optimize, due to the friction of air with the walls and the necessity to efficiently collect the air to the (compressor) exit

manifold. It is of paramount importance to have a nearly unitary efficiency in the diffuser to be competitive in the turbochargers market. For this reason, the same diffuser is used for several different compressor wheels in the most successful turbochargers. Inlet is also critical to limit and stabilize the surge curve. Most modern commercial, automotive turbocharger diffusers have nearly unitary efficiency being highly optimized through experimental tests. Invariant maps with equations to adapt the results to different input and output conditions are provided for most commercial turbochargers. Unfortunately, for the designer, the true problems come with altitude performance with very different Re and Mach numbers. In most automotive applications, it is still convenient to rely on maps that use the volumetric flow rate. This means that the map from the manufacturer is converted to the original volumetric-flow-rate/compression ratio one. In fact, compressors are volumetric machines and the "original" map has always the average inlet speed in the x-axis. As altitude and moisture varies Re and Mach speed, the efficiency values become invalid. In this case, the compressor maps move and there is the necessity to increase the maximum turbocharger rpm to optimize pressure recovery. This paper focuses on a new method to adapt compressor map to altitude and water vapor content.

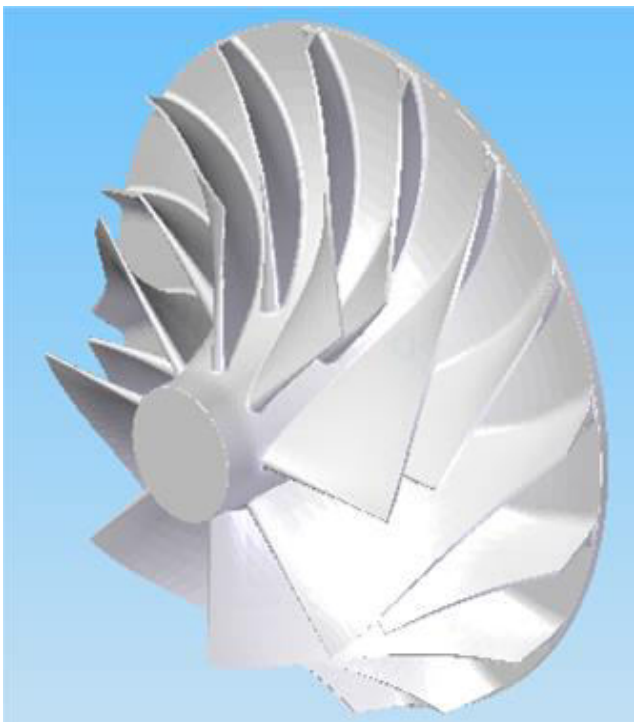

Figure-1. A 3D model of an impeller.

Table-1. Impeller data (Fig. 1-4).

# blades	**16**
External Wheel diameter	108 mm
Internal Wheel diameter	80.8 mm
A/R	0.69

EXPERIMENTAL TESTS, CFD SIMULATION AND COMMENTS ON MAPS

Experimental tests are extremely expensive, since they require a proper test rig. Therefore, in most cases, only a few points are experimentally obtained and the other are interpolated with various methods. The most "rigorous" of them is CFD (Computational Fluid Dynamics). The traditional fundamental quantities are the Mass Flow Function (*MFF*), compression ratio β, correct rotation speed ω_c and isentropic compression efficiency η. These parameters come from the conservation of mass concept. In fact, for a fluid the density and the volume change inside the compressor. For an ideal-compressible-gas in chocking, equation (1) holds for mass flow m'_{max}.

$$MFF_{\max} = \frac{\dot{m}_{\max}\sqrt{T_{0t}}}{p_{0t}} = A\sqrt{\frac{k}{R}}\left(\frac{k+1}{2}\right)^{-\frac{k+1}{2(k-1)}} \quad (1)$$

Therefore, MFF, in chocking conditions, depends only on geometry and fluid and not on the initial conditions T_{0t} and p_{0t} (total temperature and pressure). Therefore, traditionally, a corrected mass flow rate MF_c is used (2) for the x axis of the "universal" compressor map supplied by the manufacturer.

$$MFc = \frac{\dot{m}\sqrt{\frac{T_{0t}}{T_{rt}}}}{p_{0t}/p_{rt}} \quad (2)$$

In addition, the efficiency η and the compression ratio β are made independent from the inlet condition (3) (4).

$$\beta = f\left(MFc; \frac{n}{\sqrt{T_{0t}}}\right) = f\left(MFc; n_t\right) \quad (3)$$

$$\eta = f\left(MFc; \frac{n}{\sqrt{T_{0t}}}\right) = f\left(MFc; n_t\right) \quad (4)$$

The idea is to use a single map for all the initial conditions at the compressor intake. In fact, 0 stands for the reference physical state of the fluid at the compressor suction. The characteristic curves in the compressor map represent the compression ratio as the flow parameter changes, for given values of the correct speed n_t. In addition, the curves with constant efficiency are drawn, also called "islands" for their characteristic shape. It is observed that, for a given correct speed, the compression ratio decreases if the flow parameter increases. Furthermore, the flow rate that can be disposed of by the compressor can increases only until the sonic block is reached, at which the Mach speed is reached in a section of the impeller or of the diffuser. Contrary to the turbine,

where all the curves tend to overlap, the compressor graph has an "operating range" in which operation is possible, even if the maximum efficiency island is much smaller. This operating area is delimited at the top by a max shaft speed curve limited by the maximum allowable stress (some manufacturers admit an increase of 15% for short periods). On the right side, the map at the high flow rates is limited by the sonic block or choke. On the left the operating range is limited there is the phenomenon of pumping (or surge). In fact, as the flow rate decreases too much, the angle of incidence becomes too high with the detachment of the fluid vein. Unfortunately as the initial conditions are too far away from the test (or simulation) ones the curves move and the map is invalid. The corrections of equations (1-3) are not sufficient to have a true figure of compressor performance. To understand fully how a map is drawn a true example is introduced in this paper. The map, with a few limitations, can be easily evaluated with the CFD simulation. To reduce the complexity of the domain (Figure-1) and the computational time only one vane channel of the impeller is simulated. In order to proceed with the next meshing phase, it is necessary to "close" this channel with lids (surfaces) and transform it into a "solid" (Figures 2 and 3).

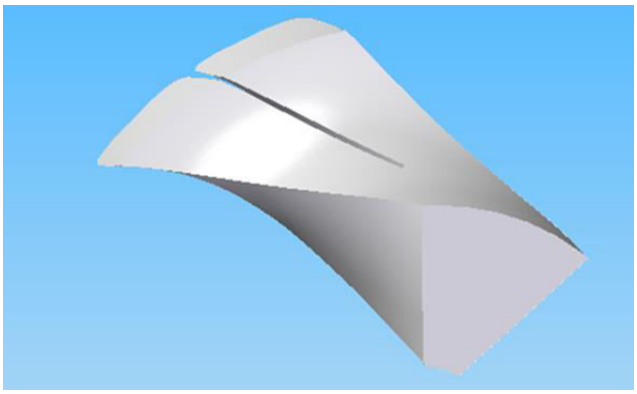

Figure-2. The 3D vane channel.

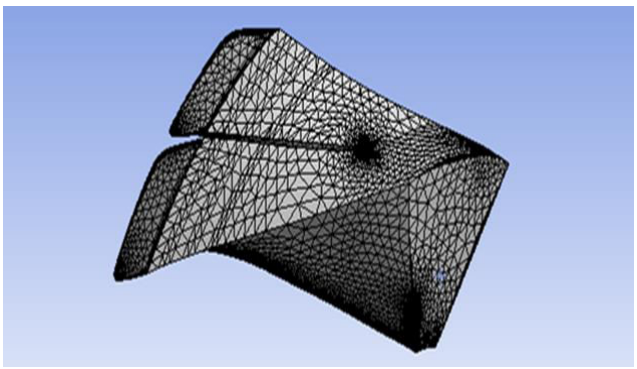

Figure-3. 3D mesh of the vane channel (406,222 elements and 122,762 nodes).

By clicking on "Boundary Conditions" button, it is possible to define the "velocity inlet" condition. This option allows, for the assigned impeller, to vary the input flow to the vane channel to draw the impeller map. In this way the only "free" parameter is the absolute input speed C_1, being the ambient air and the geometry constant. C_1 is chosen purely axial. This is an approximation, but a calculation of the speed distribution requires much longer time. At the inlet, traditionally, a static pressure of 0.93 bar is inputted for all the simulation cases. The "outflow" condition is then set on the exit surfaces. All the other surfaces of the domain are set to the condition of “Moving Wall" condition with “Rotational" movement. Numerous simulations are then carried out for four different angular velocities; in this example, of a compressor for a truck engine, the velocity set is {100,000 rpm; 88,000 rpm; 70,000 rpm; 50,000 rpm}. For each of these values, the flow rate is gradually decreased until there are anomalies of the flow exiting the impeller. Figure-4 shows the result of one of the many (13) simulations carried out: the field of motion of the relative speed is uniform and without swirling areas (Figure-3).

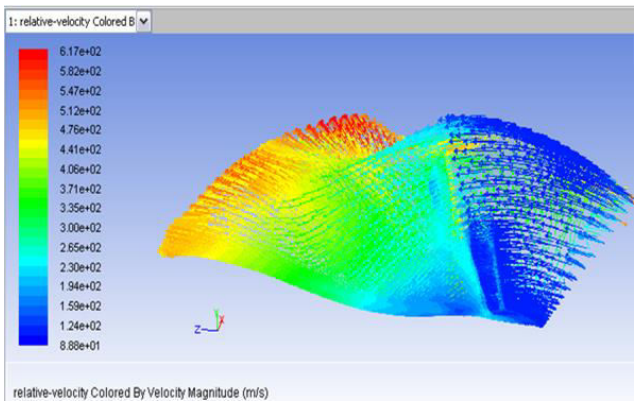

Figure-4. The velocity pattern in the 3D vane channel.

The results of the 3D simulation are summarized in Table-2.

Table-2. CFD results.

#	C_1 (m/s)	(rpm)	P_{out} (bar)	β
1	160	100,000	2.86	3.08
2	140	100,000	3	3.49
3	120	100,000	3.54	3.81
4	140	88,000	2.5	2.69
5	120	88,000	2.97	3.19
6	100	88,000	2.86	3.08
7	160	70,000	1.83	1.97
8	140	70,000	2.07	2.23
9	100	70,000	2.1	2.26
10	80	70,000	2.2	2.37
11	80	50,000	1.44	1.55
12	60	50,000	1.54	1.66
13	40	50,000	1.6	1.72

P_{out} is the total pressure with the diffuser efficiency considered as unitary**.** When designing the map of a commercial compressor, this is a common approximation, being the diffuser the difficult part to design with efficiency close to unitary. The blue curve in figure is for 100,000 rpm, while the red one is for 88,000 rpm. The curves at 50,000 and 70,000 rpm (yellow and green) are quite flat. In particular, at 70,000 rpm the compressor provides a maximum compression ratio of 2.37. As the angular speed increases, the compression ratio increases up to a value of 3.81 at 100,000 rpm. The red curve is not flat and may show an unsolved problem in the compressor design. This "critical" areas are often present in the true map, but rarely shown in the maps supplied by the manufacturers.

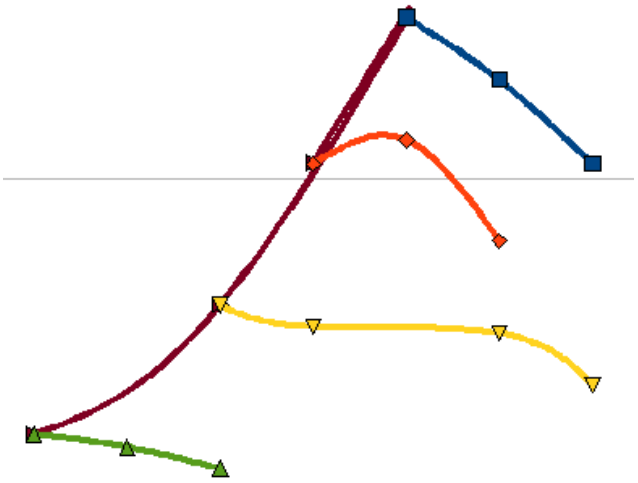

Figure-5. Graphical representation of the CFD results (numerical values in Table-2).

Figure-5 is intentionally without dimensions: in the x-axis it is possible to put and inlet speed (m/s), the Mach speed, a volumetric flow rate (m^3/s) or a normalized mass rate (kg/s) like MFF. In the y-axis, it is possible to have a total pressure, a polytrophic head or a compression ratio. The shape of the curves remains the same, being the map simply adapted to the new units. The authors usually convert the map to the units of Table-2 that is the most "raw" possible. However, this method has many limitations that are partially corrected by the "invariant" method introduced in this paper. This methods works well for automotive applications, but is less efficient at altitude where the original map is invalid. Efficiency is not difficult to evaluate. From the equation of the total pressure, it is possible to evaluate the outlet air density ρ_2, and the real output temperature T_2. At 88,000 rpm the compressor outputs a P_{total}*=2.5bar*, a P_{static}*=1.5bar* with an absolute output speed of $\boldsymbol{c_2}$*=379.4m/s* (5).

$$P_{total} = P_{static} + \frac{1}{2}\rho_2 c_2^2 \Rightarrow \rho_2 = 2\frac{P_{total} - P_{static}}{c_2^2}$$
$$T_2 = \frac{P_{static}}{R\rho_2} = 378.7K \quad (5)$$

Since it is assumed that the diffuser has unitary efficiency (with isentropic compression), it is possible to calculate the temperature of the air out of the compressor $\boldsymbol{T_3}$***=438K***. The temperature of a fully isentropic compression from inlet to outlet is T_{3iso}*=328K*. The isentropic efficiency is therefore η*=0.63* (6).

$$\eta = \frac{T_{3iso} - T_1}{T_3 - T_1} = 0.63 \quad (6)$$

Even if the method described in this paper may be questionable, a few points should be clear. The compressor map is essentially volumetric, the input data is always a speed or a volumetric flow and the output is a pressure, a pressure ratio, or a polytrophic head. Essentially, the output is energy. The flow is referred to specific ambient conditions. The simulation of the impeller is relatively easy, while the diffuser is difficult to simulate and to design properly and requires experimental tests. This is because friction plays an important role in the very critical component that should have nearly unitary efficiency. Very few points are available for drawing the map, even if the much cheaper CFD method is used. Most maps available are interpolated from few "true" points, their regularity and continuity is, in most cases, suspicious. Even the maps of the best compressors available show bumps or "difficult" point when the flow does not behave in an efficient way. The situation is aggravated by the fact that ambient conditions varies and an important role is played by the vapor content that modifies the Reynolds number and in most cases, worsens the compressor performance. This fact is well known to the people who maps piston engines where humidity is always an important data and a few map points show difficulties for unknown reasons: combustion or compressor? The tradition "invariant" axis of equations 1-4 are acceptable near test conditions, but show their huge limitations when the engines work at high altitude or use turbochargers in serial arrangement. In this case, the most common way to use maps is to reconvert them to the origin, with the volumetric flow or the inlet velocity on the x-axis. Unfortunately, output pressure (or efficiency) depends on Reynolds and Mach numbers. At altitude, the turbine works in favorable conditions while the compressor deals with rarefied air. The result is shaft over speed and higher temperature of compressed air due to reduced compressor performance and poor turbine-compressor matching.

CORRELATION OF COMPRESSION RATIO WITH MACH NUMBER

A method to correlate compression ratio with Mach number is introduced in paper [1]. The original compressor map of polytrophic head against inlet air velocity (Mach) for varying rotational speeds are used as an input to define a non-dimensional invariant performance surface (map) of head and volume flow coefficients. In this way it is possible to design new efficiency curves of polytrophic head vs. flow for a new set of inlet condition. Paper [1] claims a 3% accuracy. This method can be rearranged in equations (7) (8) (9).

$$\psi = \frac{2gH}{(\omega R)^2} \tag{7}$$

$$\phi = \frac{c_1 A}{\pi \omega R^3} = \frac{Q}{\omega R^2 U} \tag{8}$$

$$Mu = \frac{\omega R}{M} \tag{9}$$

Equation (9) [1] is the starting concept of the method. The tangential speed of the impeller is the reference Mach number *Mu* (9). A new set of curves can be drawn at constant *Mu* for each set of φ and Ψ. Given the new input velocity (or volumetric flow) and ambient conditions, equation (10) makes it possible to evaluate the Mach number *M* and *Mu* at the inlet with fair accuracy [2] (Table-3). This equation takes into account of vapor gas and $C0_2$ content in ambient air.

$$\begin{aligned} M &= a_0 + a_1 t + a_2 t^2 + (a_3 + a_4 t + a_5 t^2) x_w \\ &+ (a_6 + a_7 t + a_8 t^2) p_s + (a_9 + a_{10} t + a_{11} t^2) x_c \\ &+ a_{12} x_w^2 + a_{13} p_s^2 + a_{13} x_c^2 + a_{15} x_w p_s x_c \end{aligned} \tag{10}$$

The new total pressure can then be calculated with equation (7). The other improvements are given by equations (11) and (12) that include the "true" inlet density in equations (7-9).

$$p_{total} = \rho g H \tag{11}$$

$$\begin{aligned} \rho &= (3.48349 + 1.44(x_c - 0.0004)) \times 10^{-3} \\ &+ \tfrac{p_s}{T}(1 - 0.378 x_w) \end{aligned} \tag{12}$$

Equations (11) and (7) use the inlet air density to evaluate the total pressure. An accurate evaluation of the air density can be obtained with equation (12) [2]. The new "invariant" map starts from the concept that inlet conditions such as temperature, pressure and molecular weight have a large influence on compressor performance. If circumferential speed and Reynolds number ratio are the same for two different sets of suction conditions, then the corresponding non-dimensional map of head coefficient vs. volume flow coefficient is equivalent. Equation (11) uses the real air density $\boldsymbol{\rho}$ instead of Re. In fact, the air viscosity does not change much with altitude and the other parameters in Re are constant (geometric) or already taken into account in the inlet Mach number. The method is approximated by several factors. The most important one is that it assumes that compressor efficiency does not vary with air density. This is obviously not true. If the initial reference values at inlet are very different from the true ones then the map should be recalculated [3-25]. However, this compensation method is far better than the traditional one, being fit for most applications.

Table-3. Data of equation (10).

a0	**331.5024**	**a9**	**-85.20931**
a1	0.603055	a10	0.228525
a3	-0.000528	a11	5.91 10-5
a4	51.471835	a12	-2.835149
a5	0.1495874	a13	-2.15 10-13
a6	0.000782	a14	29.179762
a7	-1.82 10-7	a15	0.000486
a8	2.93 10-10		

CONCLUSIONS

This paper shows that the traditional method to draw compressor maps in not very efficient. It should be clear that most compressor maps are interpolated from very few CFD or experimental data. A simplified CFD method used by the Authors when the manufacturer does not supply the compressor map is introduced in this paper. The initial "measured" map has a volumetric flow rate in input (x-axis) and an absolute pressure ratio in output (y-axis). The islands of constant efficiency are then drawn onto the raw map. In most cases, the manufacturer redraws this map by replacing the x-axis with the MFF (Mass Flow Function). In this way, it is possible to use the map with different ambient (inlet) conditions. However, this method is not very efficient and large errors are introduced in the calculations. An invariant method based on the ambient sound speed (Mach) was introduced by paper [1]; this method is corrected in this paper by introducing more accurate values for density and Mach speed. The new invariant map obtained in this way can be successfully used for most automotive applications. In airplanes, however, at altitudes over 3,000m, even the new method shows its limitations, with the necessity to recalculate the maps with CFD simulation.

SYMBOLS

Symbol	Description	Unit	Value
MFc	Corrected Mass Flow	kg/s	-
MFF_{max}	Mass Flow Function choke	-	-
T_{0t}	Total ambient temperature	K	-
p_{0t}	Total ambient pressure	Pa	-
T_{rt}	Total reference temperature	K	-
p_{rt}	Total reference pressure	Pa	-
k	Specific heat ratio	-	-
n_t	Corrected compressor shaft speed	$s^{-1}K^{-0.5}$	-
C_1	Absolute average velocity at impeller inlet	m/s	-
P_{out}	Total output pressure	Pa	-
β	Compression ratio	-	-
P_{total}	Total output pressure for the example	Pa	250,000
P_{static}	Pressure out of the impeller for the example	Pa	150,000
C_2	Absolute average velocity at impeller outlet for the example	m/s	379.4
ρ_2	Volumetric mass for the example	kg m^{-3}	-
T_2	Impeller outlet air temperature for the example (5)	K	387.7
R	Ideal Gas Constant	$JK^{-1}kg^{-1}$	287
T_3	Diffuser outlet air temperature for the example (6)	K	438
T_{3iso}	Diffuser outlet air temperature for the example (6) isentropic compression	K	378.7
ρ	Volumetric mass at compressor inlet	kg m^{-3}	-
g	Gravity acc.	m/s^2	9.81
ρ	Air Density	lb/ft^3	0.0765
H	Height of the column of air with density ρ	m	-
ω	Impeller angular velocity	rad s^{-1}	-
R	Impeller outer radius	m	-
A	Compressor intake area	m^2	-
Q	Volumetric flow rate	m^3s^{-1}	-
U	Impeller tangential velocity ωR	m s^{-1}	
M	Mach number at inlet	M	
Mu	Reference Mach number	-	
φ	Generalized flow rate	-	
Ψ	Generalized head	-	
t	Inlet temperature	C	
x_w	mole fraction of water vapor in inlet air	-	
x_c	mole fraction of CO_2 in inlet air	-	
p_s	Inlet static pressure	Pa	
p_{total}	Total diffuser output pressure	Pa	
T	Inlet temperature	K	

REFERENCES

[1] A. Ravi, L. Sznajder and I. Bennett. 2015. Compressor map prediction tool. 9th International Conference on Compressors and their Systems. IOP Conf. Series: Materials Science and Engineering 90 doi:10.1088/1757-899X/90/1/012042.

[2] K. Rasmussen. 1997. Calculation methods for the physical properties of air used in the calibration of microphones. Department Of Acoustic Technology Technical University Of Denmark Report PL-11b, 1997 DTU on line library.https://orbit.dtu.dk/en/publications/calculation-methods-for-the-physical-properties-of-air-used-in-th

[3] L. Piancastelli, L. Frizziero, G. Donnici. 2015. The Meredith ramjet: An efficient way to recover the heat wasted in piston engine cooling. Asian Research Publishing Network (ARPN). Journal of Engineering and Applied Sciences. ISSN 1819-6608, 10(12): 5327-5333, EBSCO Publishing, 10 Estes Street, P.O. Box 682, Ipswich, MA 01938, USA.

[4] L. Piancastelli, L. Frizziero, G. Donnici. 2015. Turbomatching of small aircraft diesel common rail engines derived from the automotive field. Asian Research Publishing Network (ARPN). Journal of Engineering and Applied Sciences. ISSN 1819-6608, 10(1): 172-178, EBSCO Publishing, 10 Estes Street, P.O. Box 682, Ipswich, MA 01938, USA.

[5] P. P. Valentini, E. Pezzuti E. Computer-aided tolerance allocation of compliant ortho-planar spring mechanism. Int. Jou. Of Computer Applications In Technology, 53: 369-374, ISSN: 0952-8091, doi: 10.1504/IJCAT.2016.076801

[6] L. Piancastelli, S. Cassani. 2017. Maximum peak pressure evaluation of an automotive common rail diesel piston engine head. Asian Research Publishing

Network (ARPN). Journal of Engineering and Applied Sciences. ISSN 1819-6608, 12(1): 212-218, EBSCO Publishing, 10 Estes Street, P.O. Box 682, Ipswich, MA 01938, USA.

[7] L. Piancastelli, S. Cassani. 2017. Power Speed Reduction Units for General Aviation Part 2: General Design, Optimum Bearing Selection for Propeller Driven Aircrafts with Piston Engines. Asian Research Publishing Network (ARPN). Journal of Engineering and Applied Sciences. ISSN 1819-6608, 12(2): 544-550, EBSCO Publishing, 10 Estes Street, P.O. Box 682, Ipswich, MA 01938, USA.

[8] L. Piancastelli, S. Cassani. 2017. High Altitude Operations with Piston Engines Power Plant Design Optimization Part V: Nozzle Design and Ramjet General Considerations. Journal of Engineering and Applied Sciences. ISSN 1819-6608, 12(7): 2242-2247, EBSCO Publishing, 10 Estes Street, P.O. Box 682, Ipswich, MA 01938, USA.

[9] L. Piancastelli, M. Gardella, S. Cassani. 2017. Cooling System Optimization for Light Diesel Helicopters. Journal of Engineering and Applied Sciences. ISSN 1819-6608, 12(9): 2803-2808, EBSCO Publishing, 10 Estes Street, P.O. Box 682, Ipswich, MA 01938, USA.

[10] L. Piancastelli, S. Cassani. 2017. On The Conversion Of Automotive Engines For General Aviation. Journal of Engineering and Applied Sciences. ISSN 1819-6608, 12(13): 4196-4203, EBSCO Publishing, 10 Estes Street, P.O. Box 682, Ipswich, MA 01938, USA.

[11] L. Piancastelli, S. Cassani. 2017. Convertiplane Cruise Performance with Contra-Rotating Propeller. Journal of Engineering and Applied Sciences. ISSN 1819-6608, 12(19): 5554-5559, EBSCO Publishing, 10 Estes Street, P.O. Box 682, Ipswich, MA 01938, USA.

[12] A. Ceruti T. Bombardi T. and L. Piancastelli. 2016. Visual Flight Rules Pilots Into Instrumental Meteorological Conditions: a Proposal for a Mobile Application to Increase In-flight Survivability. International Review of Aerospace Engineering (IREASE). 9(5).

[13] Piancastelli L., Cremonini M., Cassani S., Calzini F., Pezzuti E. 2018. Intake and exhaust position optimization in the cooling duct of diesel helicopters ARPN Journal of Engineering and Applied Sciences. 13(17): 4811-4819.

[14] Piancastelli L., Cassani S., Pezzuti E., Pompei L. 2018. Multi-objective optimization of the cooling system of a diesel helicopter ARPN Journal of Engineering and Applied Sciences. 13(16): 4610-4616.

[15] Piancastelli L., Cassani S. 2019. Energy transfer from airborne high altitude wind turbines: Part I, A feasibility study of an autogirogenerator from an existing helicopter ARPN Journal of Engineering and Applied Sciences. 14(7): 1407-1413.

[16] Piancastelli L., Cassani S. 2019. Energy transfer from airborne high altitude wind turbines: Part II performance evaluation of a autogiro-generator ARPN Journal of Engineering and Applied Sciences. 14(17): 2972-2979.

[17] Piancastelli L., Sportiello L., Pezzuti E., Cassani S. 2019. Study and optimization of advanced heat sinks for processors ARPN Journal of Engineering and Applied Sciences. 14(5): 1082-1088.

[18] Piancastelli L., Bragaglia L., Cremonini M., Cassani S., Pezzuti E. 2018. Feasibility study of the installation of an additional "over lift" wing on the ch47 Chinook for cruise performance improvement through the lift-compound approach ARPN Journal of Engineering and Applied Sciences. 13(19): 8142-8149.

[19] Piancastelli L., Colautti D., Cremonini M., Cassani S., Torre A., Pezzuti E. 2018. Feasibility study and preliminary design of a Ram-Pulsejet for hypersonic passenger Air Transport ARPN Journal of Engineering and Applied Sciences. 13(20): 8356-8365.

[20] Piancastelli L., Bernabeo R. A., Cremonini M., Cassani S., Calzini F., Pezzuti E.2018. Optimized parachute recovery systems for remote piloted aerial systems ARPN Journal of Engineering and Applied Sciences. 13(16): 4590-4597.

[21] Piancastelli L., Pirazzini A., Cremonini M., Cassani S., Calzini F., Pezzuti E. 2018. The optimization of power generation in low-cost Massproduced wheeled wind turbines ARPN Journal of Engineering and Applied Sciences. 13(15): 4466-4474.

[22] Piancastelli L., Cassani S., Calzini F., Pezzuti E. 2018.The decisive advantage of CRDID on spark-ignition piston engines for general aviation: Propeller and engine matching for a specific aircraft. ARPN

Journal of Engineering and Applied Sciences. 13(13): 4244-4252.

[23] Piancastelli L., Errani V., Cassani S., Calzini F., Pezzuti E. 2018. An analytical solution for the determination of the loads acting on a semi-elliptical wing: The case of the Reggiane Re 2005 WWII fighter ARPN Journal of Engineering and Applied Sciences. 13(14): 4393-4400.

[24] Piancastelli L., Pezzuti E., Cassani S. 2018. Flow analysis of multiple injectors in high-power-density HSDI CR diesel engines Defect and Diffusion Forum. 388, pp. 1-13.

[25] Piancastelli, L., Cassani, S., Calzini, F., Pezzuti, E. 2018. Mobility improvement of heavy tracked vehicles: The "pan" tank experience ARPN Journal of Engineering and Applied Sciences. 13(22): 8937-8944.